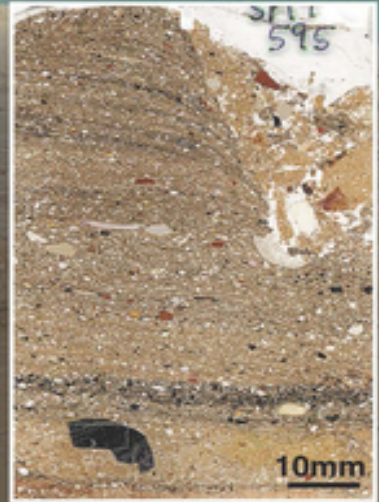
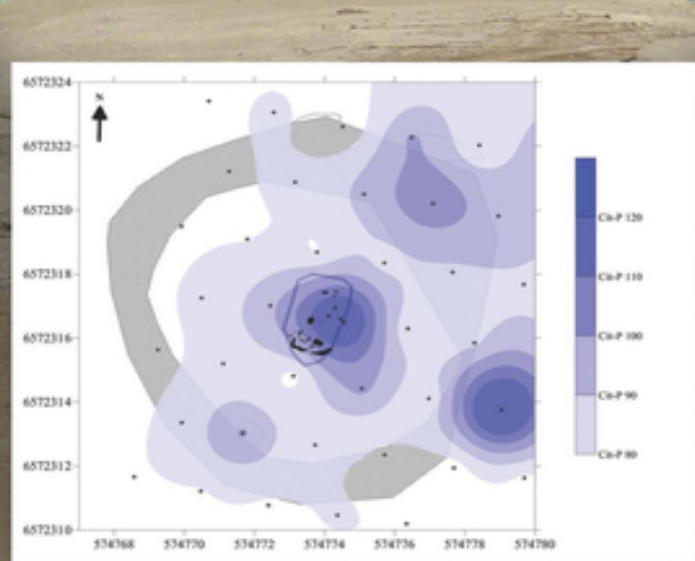
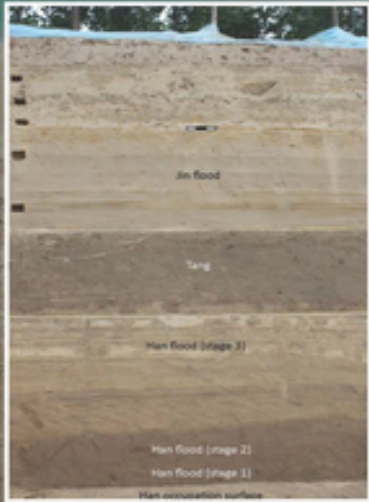


Second Edition

Practical and Theoretical Geoarchaeology

Paul Goldberg and Richard I. Macphail

Chris Carey and Yijie Zhuang



WILEY Blackwell

Table of Contents

[Cover](#)

[Title Page](#)

[Copyright Page](#)

[Dedication Page](#)

[Preface to Revised Edition](#)

[Acknowledgments](#)

[1 Introduction to Practical and Theoretical
Geoarchaeology](#)

[1.1 Introduction](#)

[2 Sediments](#)

[2.1 Introduction](#)

[2.2 Types of Sediments](#)

[2.3 Organic Matter and Sediments](#)

[2.4 Archaeological Sediments](#)

[2.5 Conclusions: Sediments vs. Soils](#)

[3 Stratigraphy](#)

[3.1 Introduction](#)

[3.2 Stratigraphy and Stratigraphic Principles](#)

[3.3 Facies and Microfacies](#)

[3.4 Correlation](#)

[3.5 Keeping Track: The Harris Matrix](#)

[3.6 Concluding Comments](#)

[4 Soils](#)

[4.1 Introduction](#)

[4.2 Soil Horizons](#)

[4.3 Differentiating Soils and Sediments](#)

[4.4 The Five Soil-forming Factors](#)

[4.5 Soil Profiles and Soil Properties](#)

[4.6 Important Soil-forming Processes](#)

[4.7 Conclusions](#)

[5 Hydrological Systems I: Slopes and Slope Deposits](#)

[5.1 Introduction to Fluvial Systems](#)

[5.2 Fluvial Landscape Studies - Slopes](#)

[5.3 Erosion, Movement, and Deposition on Slopes](#)

[5.4 Low Slope Arid Environments and Sheetwash](#)

[5.5 Conclusions](#)

[6 Rivers](#)

[6.1 Introduction](#)

[6.2 Stream Erosion, Transport, and Deposition](#)

[6.3 Stream Deposits and Channel Patterns](#)

[6.4 Floodplains](#)

[6.5 Stream Terraces](#)

[6.6 Conclusions](#)

[7 Lakes](#)

[7.1 Introduction](#)

[7.2 Origins and Types of Lakes](#)

[7.3 Characteristics of Lakes](#)

[7.4 A Short Summary of Wetland Hydrology and Soils](#)

[7.5 Geoarchaeological Examples of Lakes](#)

[7.6 Geoarchaeological Examples of Wetlands](#)

[7.7 Conclusions](#)

[8 Aeolian Environments](#)

[8.1 Introduction](#)

8.2 Aeolian Processes and Sediments

8.3 Examples of Sites in Aeolian Sand Contexts

8.4 Bioturbation in Sandy Terrains

8.5 Fine-grained Aeolian Deposits

8.6 Concluding Comments

9 Marine Coasts

9.1 Introduction

9.2 Coastal Environments

9.3 Low-energy Estuarine Mudflat and Lagoonal Environments

9.4 Salt Marsh, Mangrove, and Other Swamplands

9.5 Middens

9.6 Conclusions

10 Caves and Rockshelters

10.1 Introduction

10.2 Formation of Caves and Rock Shelters

10.3 Study of Caves and Rockshelters

10.4 Cave Deposits and Processes

10.5 Environmental Reconstruction

10.6 Methods of Study of Cave Sediments

10.7 Conclusions

11 Human Impact: Changes to the Landscape

11.1 Introduction

11.2 Forest and Woodland Clearance

11.3 Agricultural Practices

11.4 Other Managed Changes to the Landscape

11.5 Conclusions

12 Human Use of Materials

- 12.1 Introduction
- 12.2 Lithics and Ochre
- 12.3 Constructional Materials
- 12.4 Metal Working
- 12.5 Fuels and Fuel Waste
- 12.6 Concluding Remarks
- 13 Anthropogenic Deposits
 - 13.1 Introduction
 - 13.2 Concepts and Aspects of Anthropogenic Deposits
 - 13.3 New World Mounds and Monumental Earthen Architecture
 - 13.4 Settlement Archaeology
 - 13.5 Occupation Surface Deposits
 - 13.6 Final Remarks
- 14 Experimental and Ethno-Geoarchaeology
 - 14.1 Introduction
 - 14.2 Effects of Burial and Aging
 - 14.3 Experimental “Ancient Farms” and Settlements
 - 14.4 Ethno-geoarchaeology
 - 14.5 Conclusions
- 15 Geoarchaeology in Forensic Science and Mortuary Archaeology
 - 15.1 Introduction
 - 15.2 Mortuary Practices
 - 15.3 Soils and Clandestine Graves
 - 15.4 Provenancing and Obtaining Geoarchaeological Information from Crime Scenes: Methods and Approaches

15.5 Additional Potential Methods

15.6 Practical Approaches to Forensic Soil Sampling and Potential for Soil Micromorphology

15.7 Conclusions

Acknowledgments

16 Geoarchaeological Field Methods

16.1 Introduction

16.2 Sediment Stratigraphy Across Time and Space (Deposit Models)

16.3 Macro-scale Methods

16.4 Meso-scale Methods

16.5 Coring and Trenching Techniques

16.6 Describing Soils and Sediments

16.7 Collecting Samples

16.8 Integrating Samples and Proxies

16.9 Conclusions

17 Laboratory Techniques

17.1 Introduction

17.2 Physical Techniques

17.3 Microscopic Methods and Mineralogy

17.4 Thin Section Analysis

17.5 Heavy Minerals and Mineral Provenancing

17.6 Organic Residues

17.7 Instrumentation Methods: Scanning Electron Microscope (SEM), EDS, Microprobe, and Micro-FTIR

17.8 Conclusions

18 Reporting and Publishing

18.1 Introduction

- [18.2 Management, Reporting, and Publication of Archaeological Sites](#)
- [18.3 Management of Sites: Evaluation, Assessment and Reporting](#)
- [18.4 Components of Geoarchaeological Reports and Publications](#)
- [18.5 Post-excavation Reporting and Publication](#)
- [18.6 Site Interpretation](#)
- [18.7 Conclusions](#)
- [19 Concluding Remarks and the Geoarchaeological Future](#)
- [Appendix 1](#)
 - [A1.16 \(Field Methods\)](#)
 - [A1.17 \(Laboratory Methods\)](#)
- [References](#)
- [Index](#)
- [Archaeological, Geological, and Chronological Periods and Cultures](#)
- [Sites and place names](#)
- [End User License Agreement](#)

List of Tables

- [Chapter 2](#)
 - [Table 2.1 Types of sediments; consolidated \(lithified\), rock equivalents fo...](#)
 - [Table 2.2 Common minerals and rock fragments in sediments \(modified from Bo...](#)
 - [Table 2.3 Heavy mineral associations and related geological sources \(modifi...](#)

[Table 2.4 Common grain size scales used in geology and pedology.](#)

[Table 2.5a Nomenclature used to describe bedding types \(adapted from Collin...\)](#)

[Table 2.5b Nomenclature applied to describe thickness characteristics of bed...](#)

Chapter 3

[Table 3.1 Types of stratigraphic units \(modified from NASCN, 1983: table 1 ...\)](#)

[Table 3.2 Main paleomagnetic polarity events for the last 3.5 million years...](#)

Chapter 4

[Table 4.1 Soil horizons - with suggested associated major soil processes an...](#)

[Table 4.2 Soil classification \(Soil Survey Staff, 2014 ; USDA, 2014 \).](#)

[Table 4.3 Soil characteristics and preservation of artifacts and ecofacts i...](#)

[Table 4.4 White Horse Stone, Kent, UK \(Channel Tunnel Rail Link\): summary o...](#)

Chapter 5

[Table 5.1 Generalized characteristics of slope deposits \(see Figure 5.4\).](#)

[Table 5.2 Hesby, Vestfold, Norway; geoarchaeological data and land use reco...](#)

Chapter 6

[Table 6.1 Characteristics of valley sediments \(modified from Summerfield, 1...](#)

[Table 6.2 Types of river patterns and characteristics \(modified from \(Moris...](#)

[Table 6.3 Associations of archaeological material with alluvial contexts \(n...](#)

Chapter 7

[Table 7.1 Chemical classification of elements in lake sediments \(after Haka...](#)

[Table 7.2 Major evaporate minerals \(after Reineck and Singh, 1986 : table 1...](#)

Chapter 8

[Table 8.1 Classification of aeolian dunes by Livingstone and Warren \(1996 \)...](#)

[Table 8.2 Classification and illustration of major aeolian dunes types \(mod...](#)

Chapter 10

[Table 10.1 Some recent references to important caves and rockshelters discu...](#)

[Table 10.2 Types of cave sediments \(modified from Sherwood and Goldberg 200...](#)

[Table 10.3 A sampling of the more important syn- and post-depositional proc...](#)

[Table 10.4 Some of the more common authigenic minerals associated with cave...](#)

Chapter 11

[Table 11.1 Some generalizations on global cultivation arranged by period and...](#)

[Table 11.2 Whitefriars, Canterbury, Kent, UK; chemical \(excluding phosphate...](#)

[Table 11.3 Chemical and magnetic susceptibility data from the site of the D...](#)

Chapter 13

[Table 13.1 Micromorphological and macromorphological attributes from Near a...](#)

[Table 13.2 A suggested guide to settlement composition including soil micro...](#)

[Table 13.3 Components of urban stratigraphy and their potential for weather...](#)

[Table 13.4 Phases of dark earth formation elucidated from an analogue \(Post-...](#)

[Table 13.5 Åker gard, Hamark, Norway; stabling area of Iron Age long house,...](#)

Chapter 14

[Table 14.1 Wareham Experimental Earthwork; changes to the buried soil \(Macp...](#)

[Table 14.2 Wallasea Island \(River Crouch\), Essex, UK; basic soil characteri...](#)

[Table 14.3 Bulk analysis of organic matter \(LOI\), P \(2N nitric acid\), phosph...](#)

[Table 14.4 Stables \(byres\) and domestic space: a summary of characteristics...](#)

[Table 14.5 Swedish experimental soil data \(Macphail et al., 2000\); mean va...](#)

Chapter 16

[Table 16.1 Characteristics of horizontally bedded limestone \(modified from ...](#)

[Table 16.2 Characteristics of loess \(modified from \(Lillesand and Kiefer, 1...](#)

[Table 16.3 Specifications of various multispectral and hyperspectral sensor...](#)

[Table 16.4 Geophysical techniques commonly used in both geoarchaeological a...](#)

[Table 16.5 Profile description \(below\) of Southern end of wall Profile 2 Ho...](#)

[Table 16.6 Sediment and profile description of Profile 2 from Hohle Fels Ca...](#)

[Table 16.7 Summary of major alluvial units, geomorphological features and a...](#)

Chapter 17

[Table 17.1a Example of traditional grain size analyses - from different sed...](#)

[Table 17.1b Example of traditional grain size analyses - from different soi...](#)

[Table 17.1c Example of grain size analyses - from different soils, sediment...](#)

[Table 17.2 Example of multi-method bulk sample analyses \(Maya salt working d...](#)

[Table 17.3a LOI \(estimated organic matter\), fractionated phosphate and magn...](#)

[Table 17.3b Pollen analysis of a sample \(PMM42, 2.5cm, Layer 1150\) from Fry...](#)

Chapter 18

[Table 18.1a London Guildhall; Summary of analytical data for all samples \(n ...](#)

[Table 18.1b London Guildhall; Pearson product-moment correlation coefficient...](#)

Appendix 1

[**Table A1.17.5.1** Example of producing a continuous series of thin sections fr...](#)

[**Table A1.17.6.1** Suggested outline for presenting soil micromorphological inf...](#)

[**Table A17.6.2** Freshwater sediment analysis: full presentation of soil microm...](#)

[**Table A17.6.3** Soil analysis: summarized data for soil microfabric types/micr...](#)

[**Table A17.6.4** Anthropogenic sediment analysis: summarized data for soil micr...](#)

List of Illustrations

Chapter 2

[Figure 2.1 Examples of sediment types associated with archaeological sites. ...](#)

[Figure 2.2 Triangular textural diagrams showing classes of mixtures of sand,...](#)

[Figure 2.3 A graphical representation of sorting, the distribution of grain ...](#)

[Figure 2.4 Particle shape \(form\) and roundness. \(a\) Aspects of particle shap...](#)

[Figure 2.5 Surface texture of grains, illustrated here as an SEM photo of qu...](#)

[Figure 2.6 Textural and organizational aspects of clasts in fluvial conglome...](#)

[Figure 2.7 Grouping and subdivision of sedimentary beds according to grain s...](#)

[Figure 2.8 Shape characteristics of bedding and laminae](#)

[Figure 2.9 Ripple marks. Block diagrams showing two types of surface ripple ...](#)

[Figure 2.10 Examples of sedimentary structures. \(a\) Ice wedge formed in bedd...](#)

Chapter 3

[Figure 3.1 Hypothetical triptych illustrating the complexities involved in a...](#)

[Figure 3.2 Facies. \(a\) Photograph of alluvial fan in the Ka Valley of Wester...](#)

[Figure 3.3 Location of Wilson-Leonard Site, Central Texas marked with *](#)

[Figure 3.4 Schematic cross-section through Brushy Creek, showing the positio...](#)

[Figure 3.5 \(a\) Schematic view of major lithostratigraphic units and their la...](#)

[Figure 3.6 Geological evolution of Wilson-Leonard site](#)

Chapter 4

[Figure 4.1 Soil-forming processes \(Figure 4.9\), controls on soil composition...](#)

[Figure 4.2a Generalized soil profile showing bedrock \(R\), soil parent materi...](#)

[Figure 4.2b Field photo of shallow humic soil formed directly on chalk \(Rend...](#)

[Figure 4.2c Field photo of deep argillic brown earth soil profile \(Alfisol/L...](#)

[Figure 4.3a Alfisol formed on limestone under woodland in a humid western te...](#)

[Figure 4.3b Field photo, Brean Down profile, as Figures 4.3 and 4.4; at the ...](#)

[Figure 4.3c Evolutionary development of soils at Brean Down from Late Glacia...](#)

[Figure 4.3d Detail of Figure 4.3, showing Neolithic/Beaker soil development:...](#)

[Figure 4.4 Classic soils and vegetation across the globe according to climat...](#)

[Figure 4.5 The soil catena; soil drainage classes in a moist temperate envir...](#)

[Figure 4.6a Field photo, Carn Brea Neolithic settlement Redruth, Cornwall, U...](#)

[Figure 4.6b Photomicrograph of "embedded grain", a feature relict of perigla...](#)

[Figure 4.6c Scan of thin section sample M13 from buried soil 113 below a rec...](#)

[Figure 4.7 Upland soil drainage catena \(see Figure 4.5\), with plateau should...](#)

[Figure 4.7b Field photo Saddlesborough Reave-buried Cambic Stagnogley, with ...](#)

[Figure 4.7c Field photo Saddlesborough Reave-buried peat over E horizon \(Hum...](#)

[Figure 4.8 Field photo of plaggen soil, The Netherlands. Originally a podzol...](#)

[Figure 4.9a, b, and c Selected types of soil processes \(simplified\).](#)

[Figure 4.10a Photomicrograph of Late-glacial hollow infilling, associated wi...](#)

[Figure 4.10b As Figure 10a, photomicrograph of ferruginized bone cluster \(BC...](#)

[Figure 4.10c Scan of M1 1995 \(Hyena Den Cave, Wookey Hole, Somerset, UK\); La...](#)

[Figure 4.11a Field photo; Boxgrove, GTP 25; terrestrial slope solifluction d...](#)

[Figure 4.11b As Figure 4.11a, *in situ* refitting flints within the chalk pell...](#)

[Figure 4.11c As Figures 4.11a-4.11b, photomicrograph of terrestrial slope so...](#)

[Figure 4.11d As Figures 4.11a and 4.11b, photomicrograph of terrestrial slop...](#)

[Figure 4.12a Field photo of Azilian site of Rocher de l'Impératrice, Plougas...](#)

[Figure 4.12b Scan of M3/3 Rocher de l'Impératrice, Plougastel-Daoulas, Finis...](#)

[Figure 4.12c As Figure 4.11b; Photomicrograph of M3/3 \(base\); compact lentic...](#)

[Figure 4.12d As Figure 4.11d, under oblique incident light \(OIL\); note iron ...](#)

[Figure 4.13 Generalized relations between soil pH, humidity, and humus types...](#)

Chapter 5

[Figure 5.1 Pathways of water movement along slopes, and within soils and bed...](#)

[Figure 5.2 A generalized depiction of the effect of vegetation on runoff and...](#)

[Figure 5.3 Gullies formed on soft, easily erodible Pleistocene/Holocene lacu...](#)

[Figure 5.4 Colluvial soil movement down slope and down valley \(after Allen 1...](#)

[Figure 5.5a Field photo, Hesby nordre, Vestfold, Norway; toe-slope sediments...](#)

[Figure 5.5b Schematic key to Figure 5.2a; 1 - topsoil, 2-3 - medieval soil, ...](#)

[Figure 5.5c Hesby nordre, Vestfold, Norway: Geochemical log of P, LOI, and m...](#)

[Figure 5.6 Ashcombe Bottom section drawing \(courtesy of Mike Allen\) showing ...](#)

[Figure 5.7 Strawberry Hill, Wiltshire, England; plan and section of colluvia...](#)

[Figure 5.8a Scan of M56 \(steep-sided Lågen River valley, Fryasletta, Oppland...](#)

[Figure 5.8b Photomicrograph of M56, Layer 1146 \(Figure 5.8a\); mass-movement, ...](#)

[Figure 5.9a Field photo of excavations ahead Bergen-Fløen rail tunneling, Be...](#)

[Figure 5.9b Field photo, as Figure 5.9a, but further upslope and up in the s...](#)

[Figure 5.9c Field photo, as Figure 5.9b, but lateral examples of deposits at...](#)

[Figure 5.9d Scan of thin section 50137A from Profile C2031 \(Figure 5.9c; Lay...](#)

[Figure 5.9e Photomicrograph of M50137A \(Layers 6/12\); silt loam and silt lay...](#)

[Figure 5.9f As Figure 5.9e, under OIL.](#)

[Figure 5.10a Field photo; Djibouti, sheetwash sand and gravel-covered low sl...](#)

[Figure 5.10b Scan of thin section M1B; note junction between calcareous fine...](#)

[Figure 5.10c Photomicrograph of M1B; quartz sand, sand-size calcareous sedim...](#)

[Figure 5.10d As Figure 5.10c, under OIL; opaque minerals are magnetite and f...](#)

Chapter 6

[Figure 6.1 Bedforms in relation to grain size \(mostly sand\) and stream power...](#)

[Figure 6.2 Hjulström's diagram showing velocity associated with the erosion,...](#)

[Figure 6.3 \(a\) Different fluvial channel pattern types showing the interrela...](#)

[Figure 6.4a Braided channel during a flood in the Gebel Katarina area, south...](#)

[Figure 6.4b Braided channel from Qadesh Barnea area, Sinai. The braided chan...](#)

[Figure 6.5 Block diagram showing surface morphology of a braided stream with...](#)

[Figure 6.6 Coarse alluvium exposed at surface of an alluvial fan in south-we...](#)

[Figure 6.7 \(a\) Block diagram illustrating the major features of a meandering...](#)

[Figure 6.8 \(a\) Stratigraphy at Sanyangzhuang showing anthropogenic paleosols...](#)

[Figure 6.9 Lateral variations in deposits and facies are clearly shown in th...](#)

[Figure 6.10 Changes of positions of meanders within the Red River during the...](#)

[Figure 6.11 Photograph of late Holocene floodplain Ford alluvium from Cowhou...](#)

[Figure 6.12 Section through charcoal and burned soil-rich remains of prehist...](#)

[Figure 6.13 \(a\) SEM X-ray backscatter image of HWK M26A \(Layer 2 Lower\); bon...](#)

[Figure 6.14 Digital Elevation Model \(DEM\) around the Sutlej-Yamuna interfluv...](#)

[Figure 6.15 Photo of terraces from Nahal Ze'elim, western Jordan Valley. Thi...](#)

[Figure 6.16 Idealized view of alluvial terrace formation developed in alluvi...](#)

[Figure 6.17 Alluvial sequences from several drainages in south-western Arizo...](#)

[Figure 6.18 Composite cross-section from Middle Gila River, AZ, illustrating...](#)

[Figure 6.19 Histograms showing number of radiocarbon dates for alluvial fill...](#)

[Figure 6.20 \(a\) Google Earth image showing the location of the Longwangchan ...](#)

[Figure 6.21 Schematic illustration showing locations of Neolithic, Bronze Ag...](#)

[Figure 6.22 \(a\) Spatial boundaries of different geomorphological types in th...](#)

[Figure 6.23 Schematic summary of the types of archaeological context that ca...](#)

[Figure 6.24 Nahal Zin area in the Central Negev, Israel. The Upper Paleolith...](#)

[Figure 6.25 Nahal Zin valley looking SW toward the Central Negev Plateau fro...](#)

[Figure 6.26 Schematic W-E cross-section across Nahal Zin showing the topogra...](#)

[Figure 6.27a The site of Boker Tachtit as seen from the site of Boker. The t...](#)

[Figure 6.27b The terrace sediments of Boker Tachtit are composed of two majo...](#)

[Figure 6.28a The site complex of Boker, situated on the west bank of Nahal Z...](#)

[Figure 6.28b Area BE of the original excavation. Layers of pale, brown-color...](#)

[Figure 6.28c Detail of profile shown in Figure 6.28b showing the alternation...](#)

[Figure 6.29 Generalized cross-section through Nahal Zin showing the changes ...](#)

Chapter 7

[Figure 7.1 Zonation and terminologies used to designate different regions in...](#)

[Figure 7.2 Illustration demonstrating transportation processes to, within, a...](#)

[Figure 7.3 External and internal factors on sedimentation in a lake system. ...](#)

[Figure 7.4 Simple schematic diagram illustrating hydrological processes asso...](#)

[Figure 7.5 Triangular diagram for classification of lakes based on water los...](#)

[Figure 7.6 Terminologies and classification of erosion and deposition proces...](#)

[Figure 7.7 Field photograph of tilted sediments from 'Ubeidiya Formation, Jo...](#)

[Figure 7.8 Reconstruction based on micromorphology of the sedimentary enviro...](#)

[Figure 7.9 Photomicrograph of Boxmoor pingo pond fill, Hertfordshire, UK; PE...](#)

[Figure 7.10 \(a\) Sea level curve for the southern Yangtze delta from 8700 to ...](#)

[Figure 7.11 Wooden structure showing a possibly wooden wall outside raised f...](#)

[Figure 7.12 \(a\) Profile showing the grayish-darkish later period paddy field...](#)

Chapter 8

[Figure 8.1 Distribution of sandy and silty aeolian deposits over the globe...](#)

[Figure 8.2 Diagram showing the relationship of particle size in mm to thresh...](#)

[Figure 8.3 Schematic view of aeolian transport of sediment grains](#)

[Figure 8.4 Erosional effects of the wind: \(a\) ventifacts from the Western De...](#)

[Figure 8.5 Sites and aeolian deposits in the Sinai and Negev Deserts. \(a\) Sa...](#)

[Figure 8.6 Loess deposits. \(a\) Section of loess and paleosols in an upland p...](#)

[Figure 8.7 Two views of sediments in the Hamifgash area, the confluence of N...](#)

[Figure 8.8 The hammer here is resting on the remains of cross-bedded sandy d...](#)

[Figure 8.9 \(a\) Google Earth image detail of Negev and Sinai showing linear d...](#)

[Figure 8.10 Dunes and stratification. \(a\) Major dune types with arrows repre...](#)

[Figure 8.11 Barchan dune. \(a\) Photograph of barchan dune in Sinai, Egypt. No...](#)

[Figure 8.12 Geomorphic evolution of Northern Sinai and the Western Negev, sh...](#)

[Figure 8.13a The original cutting of GMX at Gwithian showing the key Phases ...](#)

[Figure 8.13b The criss-crossing ard marks preserved at the base of layer 5,...](#)

[Figure 8.13c The preservation of spade marks in phase 5 again attest to the ...](#)

[Figure 8.14 Distribution of major loess deposits in the world](#)

[Figure 8.15 Generalized model showing methods of transport and deposition of...](#)

[Figure 8.16 Mechanisms of dust entrapment and accumulation](#)

[Figure 8.17a Thick sequence of loess deposits interspersed with simple and c...](#)

[Figure 8.17b Thick accumulation of loess blanketing the landscape in Uzbekis...](#)

[Figure 8.18 Stratigraphic drawing of loess section from Moldova V \(Ukraine\)...](#)

Chapter 9

[Figure 9.1a Reconstruction of Middle Pleistocene paleo-coastline at Boxgrove...](#)

[Figure 9.1b Field photo of Boxgrove paleobeach at GTP 25, looking "sewards"...](#)

[Figure 9.1c Field photo, Boxgrove *in situ* flint scatter Unit 4b, mudflat and...](#)

[Figure 9.1d Photomicrograph of Unit 3 – fine beach sands with intercalated s...](#)

[Figure 9.1e As Figure 9.1b, photomicrograph of flint flake within the scatte...](#)

[Figure 9.1f As Figure 9.1d, but under crossed polarized light \(XPL\) showing ...](#)

[Figure 9.2 Diagram showing possible coastal zones – high-energy cliff/beach ...](#)

[Figure 9.3 Section across cliff/beach zone showing sediment lithology, featu...](#)

[Figure 9.4 Scan of M616333 \(Brekstad, Ørland, near Trondheim, Norway; Site D...](#)

[Figure 9.5 Field photo of Arene Candide, Liguria, Italy; 19th century photo ...](#)

[Figure 9.6 Field Photo of Vanguard Cave, Gibraltar, Upper Area B; blown dune...](#)

[Figure 9.7 Estuarine environment and land-use – Later Bronze and Earlier Iro...](#)

[Figure 9.8 Low-energy estuarine mudflat and lagoonal environments: sediment ...](#)

[Figure 9.9 Westward Ho!, Devon, UK; section drawing through estuarine sedime...](#)

[Figure 9.10 Field photo of living stromatolites at Hamelin Bay, Western Aust...](#)

[Figure 9.11a Estuarine inundation silts burying prehistoric old ground surfa...](#)

[Figure 9.11b Photomicrograph of Blackwater: “subsoil” \(300–370 mm depth\) at ...](#)

[Figure 9.11c As Figure 9.11b, under XPL; note moderately well-oriented void ...](#)

[Figure 9.12a Photomicrograph of M11971
\(Medieval Oslo, Norway; Profile 11498...\)](#)

[Figure 9.12b Photomicrograph of M2267 \(Middle
Neolithic Korsmyra in Bud, Mør...](#)

[Figure 9.12c As Figure 9.12c, under OIL.](#)

[Figure 9.12d Photomicrograph of M11957-2
\(Sondre gate, Trondheim, Norway; Co...](#)

Chapter 10

[Figure 10.1 Rockshelters. \(a\) Laugerie Haute
\(Dordogne France\) with smooth r...](#)

[Figure 10.2 Caves. \(a\) Hayonim Cave \(Israel\) in
center with remains of colla...](#)

[Figure 10.3 Schematic representation of the types
of processes operating in ...](#)

[Figure 10.4 Eboulis from the Middle Paleolithic site
of Pech de l'Azé IV, Fr...](#)

[Figure 10.5 Pinnacle Point Cave 13b \(South Africa\).
showing calcite-indurated...](#)

[Figure 10.6 Middle Paleolithic deposits at Hayonim
Cave \(Israel\). The geolog...](#)

[Figure 10.7 Anthropogenic deposits \(a\) Photo of
anthropogenic remains in Mid...](#)

[Figure 10.8 Zhoukoudian, Locality 1. \(a\) Putative
hearth from Layer 10. The ...](#)

[Figure 10.9 Kebara Cave, looking east toward the
junction of Mt. Carmel the ...](#)

[Figure 10.10 \(a\) Plan view of Kebara Cave showing
excavations and location o...](#)

[Figure 10.11 Features associated with *in situ* burning at Kebara. \(a\) The sou...](#)

[Figure 10.12 Dumped ash accumulations. \(a\) ~80 cm-thick accumulation of bedd...](#)

[Figure 10.13 Laminated Middle and Upper Paleolithic deposits. \(a\) Shown here...](#)

[Figure 10.14 Post-depositional modifications. Remains of compressed hearths ...](#)

Chapter 11

[Figure 11.1 Tree-throw: modern example from the “hurricane” of 1987 that pro...](#)

[Figure 11.2 Tree-throw subsoil hollow \(section and part plan\) formed by a “b...](#)

[Figure 11.3a A section through Hazleton long cairn and its buried soil, show...](#)

[Figure 11.3b Photomicrograph of the “Atlantic Period” subsoil at Hazleton \(F...](#)

[Figure 11.4a Field photo of charcoal-rich Neolithic old land surface \(OLS\) t...](#)

[Figure 11.4b Photomicrograph of Neolithic old land surface \(Figure 9.4 OLS\) ...](#)

[Figure 11.5 Prehistoric \(alluvium-buried\) paleo-landscape at Raunds, Nene va...](#)

[Figure 11.6a Raunds: section through 2.5-3.0 m wide tree-throw hole \(see Fig...](#)

[Figure 11.6b Photomicrograph of burned soil in tree-throw pit, where the soi...](#)

[Figure 11.7 Model of tree-throw field soil features; \(a\) broadleaved woodlan...](#)

[Figure 11.8a Beaker cultivation at Ashcombe
Bottom: plan and section of poss...](#)

[Figure 11.8b Photomicrograph of suggested Beaker
Period ard-ploughed colluvi...](#)

[Figure 11.9a Schematic diagram of thin section
samples 1-3 and their soil mi...](#)

[Figure 11.9b Photo micrograph of vivianite \(Viv\)
phosphate nodule in manured...](#)

[Figure 11.9c As Figure 9b, under OIL.](#)

[Figure 11.9d SEM/EDS X-ray backscatter image of
phosphate nodule in Figure 9...](#)

[Figure 11.9e X-ray spectrum of phosphate nodule in
Figure 9b; typically nodu...](#)

[Figure 11.10a Field photo of example of \(plaggen-
like\) cultural soil profile...](#)

[Figure 11.10b Geochemical profile through
plaggen-like Iron Age to Migration...](#)

[Figure 11.10c As Figure 11.10a, photomicrograph
of clearance soil, character...](#)

[Figure 11.10d As Figure 11.10c , illustrating
concentration of burned sands ...](#)

[Figure 11.10e As Figure 11.10a, photomicrograph
of manured soil at around 10...](#)

[Figure 11.11 Fe \(Figure 11.11a\) and P \(Figure
11.11b\) microprobe element map...](#)

[Figure 11.12a Las Capas, Arizona, USA. Scan of
LC-M2, showing erosive and no...](#)

[Figure 11.12b As Figure 11.12a. Scan of LC-M9
\(planting hole\) and showing th...](#)

[Figure 11.13a Madjān canal, Merv, Turkmenistan. Scan of 028-56; fine sedimen...](#)

[Figure 11.13b As Fig 11.13a. Photomicrograph of 028-56; upward-fining lamina...](#)

[Figure 11.13c Datalog \(% LOI, phosphate-P, and magnetic susceptibility % \$\chi\$...](#)

[Figure 11.14 Eroded landscape at Las Médulas León, Spain brought about by Ro...](#)

Chapter 12

[Figure 12.1 Thin section scan of hearth complex from the Middle Paleolithic ...](#)

[Figure 12.2-4: Mesolithic Haakonshellaveien, Bergen, Norway; photomicrograph...](#)

[Figure 12.3 Example of colorless feldspathic microdebitage, within floor dep...](#)

[Figure 12.4 As Figure 12.3, under OIL; note white calcined bone fragment.](#)

[Figures 12.5-12.7: Early Mesolithic Lillsjön, Pengsjö i Ångermanland, Sweden...](#)

[Figure 12.6 Photomicrograph of sands and opaque ochre. PPL, frame width is ~...](#)

[Figure 12.7 As Figure 12.6, under OIL, illustrating typical orange-red ochre...](#)

[Figure 12.8a Field photo of Angkor Thom city wall, Cambodia, constructed of ...](#)

[Figure 12.8b Close-up of Figure 12.8a, showing laterite blocks with presumed...](#)

[Figure 12.9 Field photo of Angkor Thom Temple. There is a core of laterite b...](#)

[Figure 12.10 Traditional use of mud brick in rural areas of abandoned house ...](#)

[Figure 12.11 Field photo at Skálholt Ecclesiastical Center, Iceland; reconst...](#)

[Figure 12.12 Umeå University ancient farm \(Bagböle\), north Sweden, 1994; tur...](#)

[Figure 12.13 Diagrammatic section through the Umeå experimental turf roof \(c...](#)

[Figure 12.14 Field photo; Courage Brewery site, Southwark, London; upstandin...](#)

[Figure 12.15 Photomicrograph of typical compact fine sandy silt loam brickea...](#)

[Figure 12.16a An example of plant-tempered burned daub from Ecsegfalva, Earl...](#)

[Figure 12.16b Burned adobe from an Iron Age house from el Cerro de la Gavia,...](#)

[Figure 12.17 Scan of 15 cm-long impregnated block \(M18\) at Huizui, Henan Pro...](#)

[Figure 12.18 Schematic section through wall mortar, plaster and painted surf...](#)

[Figure 12.19 Photo of translucent Roman windows composed of selenite \(gypsum...](#)

[Figure 12.20 Field photo; Colchester House \(PEP89\), City of London. In this ...](#)

[Figure 12.21 Field photo; Roman London Arena, London Guildhall; dark earth o...](#)

[Figure 12.22 Scan of Roman London Arena sand layers \(Figure 12.20\), London G...](#)

[Figure 12.23 Photomicrograph of mortar building waste from the reconstructio...](#)

[Figure 12.24 As Figure 12.23, under OIL; rubified sands, grayish yellowish l...](#)

[Figure 12.25 Photomicrograph of mortar from the façade of the Alamo, San Ant...](#)

[Figure 12.26 As Figure 12.25, under XPL; note rare quartz silt component and...](#)

[Figure 12.27 Scan of medieval floor layers at Odense, Funen, Denmark, compri...](#)

[Figure 12.28 Photomicrograph of suggested weathered lime plaster floor at Od...](#)

[Figure 12.29 As Figure 12.28, under OIL; note yellowish gray colors and smal...](#)

[Figure 12.30 Photomicrograph of medieval urban deposits in the Torvet distri...](#)

[Figure 12.31 As Figure 12.30, under OIL.](#)

[Figure 12.32 As Figure 12.31; SEM/EDS X-ray backscatter image. Spheroidal "p...](#)

[Figure 12.33 As Figure 12.32, X-ray spectrum of spheroidal prill in 13.32, r...](#)

[Figure 12.34 Photomicrograph of medieval urban deposits in the Torvet distri...](#)

[Figure 12.35 As Figure 12.34, under OIL, showing red and greenish colors. Gl...](#)

[Figure 12.36 Stanford Wharf, Thames Estuary, Essex, UK. Photomicrograph of '...](#)

[Figure 12.37 Scan of M4240A1 \(large 'Green Glaze' fragment\) composed of plan...](#)

[Figure 12.38 Detailed microprobe map area \(see Fig 12.37\); Na \(sodium\) is sp...](#)

[Figure 12.39 As Fig 12.37; Cl - chlorine also appears to be focused on the s...](#)

[Figure 12.40 As Fig 12.37; Fe - iron is most strongly concentrated along the...](#)

Chapter 13

[Figure 13.1 Byblos, Lebanon. \(a\) An example of 3rd millennium BC\(?\) tell dep...](#)

[Figure 13.2a Field photo; Chalcolithic \(4700-4000 Cal BC\) tell site of Bordu...](#)

[Figure 13.2b Field photo; Borcea River terrace alluvium forming island upon ...](#)

[Figure 13.2c As Figure 13.2b, scan of M2 illustrating massive bedded alluviu...](#)

[Figure 13.2d As Figure 13.2c, photomicrograph of M2; burrowed alluvial coars...](#)

[Figure 13.2e Field photo of anthropogenic deposits at Bordușani-Popină, Area...](#)

[Figure 13.2f As Figure 13.2e \(Deposits Number 3\), photomicrograph of M15C \(s...](#)

[Figure 13.2g As Figure 13.2e \(Deposit Number 4\); photomicrograph of burned-d...](#)

[Figures 13.3a-13.3e Figs 13.3a-3e: Ashed and oxidised stabling remains from ...](#)

[Figures 13.3b-13.3c Photomicrographs of junction between stable floor “crust...](#)

[Figures 13.3d-13.3e Oxidized Atzmaut rock shelter stabling deposits originat...](#)

[Figure 13.3d Atzmaut rock shelter: Early Bronze Age levels are composed of u...](#)

[Figure 13.3e Detail of Figure 13.3d, under XPL: note abundant calcite “dung”...](#)

[Figure 13.4a Diagrammatic representation of site formation process at the Mo...](#)

[Figure 13.4b XRD \(X-ray diffraction\) analysis of the phosphate-cemented orga...](#)

[Figure 13.5a Åker gård, Hamar, Norway; Norwegian Iron Age \(6th-8th C AD “Mig...](#)

[Figure 13.5b As 13.5a, under OIL; note siliceous \(colorless\) spherule \(1\) an...](#)

[Figure 13.5c SEM X-ray backscatter image of iron flakes - hammerscale. Scale...](#)

[Figure 13.5d EDS X-ray spectrum 1 shown in 13.5c; 100% FeO.](#)

[Figure 13.6a Regional map showing location of Belize and Spanish Period site...](#)

[Figure 13.6b Aerial photograph of Marco Gonzalez, looking south-west, showin...](#)

[Figure 13.6c Field photo of Op 13-1 \(Str 14\), east face, showing monolith sa...](#)

[Figure 13.6d Reconstructed cached Early Classic basal-flange bowl \(390/1\) fo...](#)

[Figure 13.6e Scan \(M4D\); Early Classic levels \(MG 383\) are composed of a wea...](#)

[Figure 13.6f Photomicrograph of M4D \(Figure 13.6e\), illustrating waterlaid a...](#)

[Figure 13.6g Scan of thin section M3B \(Str 14, Op 13-1; west face; Figure 13...](#)

[Figure 13.7a Field photo of labeled Op 13-3 \(Str 8\), showing monoliths and Co...](#)